Quantification of Calcification in Atherosclerotic Lesions

Catherine L. Higgins, Seth A. Marvel, Joel D. Morrisett

***Abstract*—**Calcification can be deposited throughout the vasculature in several forms of calcium phosphate, including calcium hydroxyapatite (CHA). Calcium accumulation in arteries by mineralization and calcium loss from bone by osteoporosis often coexist, and vascular calcification may share common mechanisms with bone remodeling. Deposition of calcification in valves and arteries diminishes the valvular or arterial wall elasticity, a major cause of aneurysm and stenosis. Obstruction of arteries by calcification and other components can lead to heart attack and stroke. Mineralization in the femoral arteries can cause intermittent claudication in the legs, causing decreased mobility. Accurate measurement of calcification is essential for identifying other factors associated with this process and ultimately for elucidating the mechanism(s) of calcification. A wide range of methods for visualizing and measuring calcification for diagnosis and treatment in vivo and for studying the calcification process ex vivo are available. This review provides a critical comparison of older established methods and newer evolving technologies for quantifying calcification. **(*Arterioscler Thromb Vasc Biol*. 2005;25:1567-1576.)**

Key Words: calcification ■ atherosclerosis ■ MRI, micro-computed tomography ■ ultrasound

Calcium and phosphorus are the most abundant minerals in the body and are involved in a wide range of biochemical pathways, but mostly in the formation of calcium hydroxyapatite (CHA; $Ca_{10}(PO_4)_6(OH)_2$). Although CHA is the major natural component of bones and teeth, it can also deposit along with other forms of calcium phosphate in the vasculature with adverse affects. This type of deposit, known as vascular calcification, can ultimately lead to blood vessel stenosis, ischemia, and death. Approximately 90% of patients with cardiovascular disease (CVD) have vascular calcification. Because CVDs are the leading cause of death in the United States, there is considerable interest in understanding the mechanism(s) of vascular calcification and the implications for CVD.

Healthy bone exists in a dynamic state of remodeling, requiring osteoblasts that build bone under alkaline conditions and osteoclasts that degrade it under acidic conditions.[1] Cytokines, such as bone morphogenetic proteins (BMPs), interleukin-6, insulin-like growth factor-1, as well as various hormones, regulate bone remodeling.[2] As a consequence of remodeling, bone calcium and phosphate turnover occurs. In this turnover process, resorbed minerals are used to regenerate bone. When the calcium lost in degradation exceeds the calcium deposited in remodeling, there is a net loss of bone mass. With increasing age, the rate of bone degradation exceeds the rate of formation, resulting in osteoporosis, particularly in postmenopausal women, with decreased estrogens, which inhibit cytokines.[3] Some of the calcium and phosphate mobilized by remodeling may become deposited in the arterial wall, leading to atherosclerosis in ≥1 arterial bed.

CHA is the most stable form of insoluble calcium phosphate.[4] Under biological conditions, formation of CHA proceeds through noncrystalline amorphous calcium phosphate (ACP), which is stable under alkaline conditions (pH ≥8). Formation of ACP and CHA can be inhibited by many ions and other factors at their normal tissue concentrations. Osteoblast activity regulates formation of CHA, and alkaline phosphatase, which operates under alkaline conditions, is a marker for formation of ACP and its conversion to CHA.[4]

Although the mechanism of nucleation of ACP and its conversion into CHA in bone mineralization is not entirely clear, some factors of the process are known. ACP is isothermally metastable compared with the more ordered CHA. Initial mineral deposits are associated with membrane vesicles and specific bone-associated proteins such as osteonectin, osteocalcin, and matrix γ-carboxy glutamate (Gla) protein.[2,5] On nucleation, growth of CHA crystals requires increased concentrations of Ca^{2+} and PO_4^{3-} ions.[6] The transformation of ACP to CHA in vitro occurs at slightly alkaline pH (≈7.4 to 7.8) and is temperature and time dependent, suggesting that the process is autocatalytic.[7]

Presumably, decomposition of CHA in bone to its constituent ions follows the reverse process. Osteoclast activity, inhibited by increased Ca^{2+} concentrations, involves resorption and phagocytosis of calcium phosphate in an environment made acidic by carbonic anhydrase.[8,9] Osteoclasts form tunnel capillaries into the bone.[1] Interfacing with the bone surface is a ruffled border, one of the domains into which the osteoclast plasma membrane is divided.[10] Formation of a sealed compartment between the ruffled border and bone

Original received February 10, 2005; final version accepted May 11, 2005.
From the Departments of Medicine and Biochemistry/Molecular Biology, Baylor College of Medicine, Houston, Tex.
Correspondence to Dr Joel D. Morrisett, The Methodist Hospital, A601, 6565 Fannin St, Houston, TX 77030. E-mail morriset@bcm.tmc.edu

Arterioscler Thromb Vasc Biol. **is available at http://www.atvbaha.org** **DOI: 10.1161/01.ATV.0000172017.79441.73**

Comparison of Methodologies for Calcification Quantitation

Methods	Characteristics
In vivo analysis	
Ultrasonography (US)	
B-mode US	Noninvasive Qualitative visualization
IVUS	Invasive For use in patients with stable plaques only Enables localization and semiquantitation of calcification
EBCT	Noninvasive Patient exposed to radiation Enables quantitation and localization of calcification Some other plaques components can be visualized using contrast dyes
MRI	Noninvasive Enables quantitation of plaque dimensions and components including calcification Enables 3D image reconstructions of tissue (1- to 3-mm interplane resolution)
Ex vivo analysis	
μCT	Rapid Enables 3D image reconstructions of tissue (0.3- to 0.5-mm interplane resolution) Enables quantitation of calcification but not other plaque components
MRI	Enables quantitation of plaque dimensions and components including calcification Enables 3D image reconstructions of tissue (0.5- to 1.0-mm interplane resolution)
^{31}P MRS	Rapid quantitation of phosphorus P-Ca stoichiometry used to determine calcification content Sample size <1 cm^3 Tissue morphology altered during sample preparation
Tissue digital photography	Documents tissue features and components often lost in processing Does not allow tissue component quantitation
Histology	Stained sections useful for identifying plaque components and their distribution Paraffin and frozen sections often lose calcification in processing Plastic embedded tissues retain calcification allowing its quantitation
Chemical analysis	Atomic absorption, phosphomolybdate, cresolphtahlein, Fura and Indo Enables quantitation of phosphorus or calcium dyes Stoichiometry used to calculate calcification content

surface results in an acidic compartment in which CHA crystals disintegrate.[4] Subsequently, the crystals are fragmented, transported through the osteoclast by a transcytotic vesicle, and exported to the vasculature.[10]

Vascular calcification is a well-ordered, regulated process similar to mineralization of bone tissue.[11] Modulation of this process includes apoptosis of vascular smooth muscle cells (VSMCs), cell–cell interactions (macrophages and VSMCs), lipids, and plasma inorganic phosphate (P_i) levels.[2] Four types of vascular calcification have been identified: atherosclerotic (fibrotic), cardiac valve, medial artery, and vascular calciphylaxis.[2] In the atherosclerotic type, calcification initially occurs in the necrotic core of the plaque, and these types of lesions typically occur in or near bifurcations of arteries.[2] Mechanical stressors and inflammation exacerbate cardiac valve calcification. Medial artery calcification often occurs in the femorals and is characteristic of diabetes and end-stage renal disease.[2] Vascular calciphylaxis, or soft tissue calcification, is associated with a serum calcium–phosphate solubility product (K_{sp}) >60 mg^2/dL^2.[2] The extent of calcification is strongly associated with stroke, amputation, and cardiovascular mortality.[2]

Calcification in atherosclerotic lesions involves factors important for bone mineralization, including matrix vesicles, BMP-2, osteopontin, osteocalcin, and collagen I.[2] However, a major difference between vascular calcification and bone mineralization is the presence of oxidized lipids in the former but not the latter.[12] The accumulation of oxidized lipids in the subendothelial space of arteries promotes arterial calcification, whereas these lipids in skeletal bone inhibit bone formation, suggesting another link between osteoporosis and vascular calcification.[13]

Osteoprotegerin, which protects against osteoporosis, forms a perimeter around calcified lesions.[14] This protein is also in equilibrium with receptor activator of nuclear factor kappa and receptor activator of nuclear factor kappa ligand, which regulate the transition of preosteoclasts to fully differentiated osteoclasts.[15] Several current investigations are focused on elucidating the mechanism(s) of vascular calcification. An important aspect of the task is quantification of arterial calcification.

The major objective of this review is to critically evaluate the diversity of methods available for quantifying calcification by in vivo and ex vivo methods (Table). Whereas in vivo methods are used primarily for clinical assessment and treatment of CVD, ex vivo methods are critical to mechanistic studies. Among ex vivo analytical methods, cadaveric carotid arteries (CCAs) and carotid endarterectomy (CEA) tissues

have been studied for measuring calcium content. The wide variety of approaches enables comprehensive study of calcification quantification.

In Vivo Analysis

Detecting lesions in vivo has clinical importance for diagnosis and treatment as well as in research. These in vivo methods of quantifying calcification will be discussed with regard to their methodology, practice, capabilities, and limitations.

Ultrasonography

Ultrasonography (US) involves the transmission of high-frequency sound waves (2 to 10 MHz) through an anatomic site of interest followed by conversion of echoes into electrical impulses, producing 2D images. Different modes and types of US are used in echocardiography: brightness or B-mode, motion or M-mode, spectral Doppler, and color flow mapping.

B-mode US produces a gray-scale image with good anatomic detail of the ventricular septum, ventricular free walls, heart valves, papillary muscle, and chordae tendineae. Using B-mode US to evaluate carotid plaques, weak reflections (echolucent) have been associated with a higher risk of neurological events than plaques giving strong reflections (echorich).[16] Echolucent plaques have higher content of lipid and hemorrhage than echorich plaques, which usually contain more calcification and fibrous tissue.[16] Arterial ulceration is sometimes assigned incorrectly to pits in fibrotic plaque, 2D calcification with shadowing, atheromatous debris, or ulcerated plaque hemorrhage.[17] B-mode US has been used extensively to determine carotid intimal-medial far-wall thickness[18–20] and calcification. Plaque calcification can be identified by a bright, hyperechogenic area resulting in cone-shaped echo shadowing. Such qualitative imaging was used in a study of calcification in atherosclerotic plaques in association with polymorphisms of the human matrix Gla protein (MGP) gene, which codes for a protein that inhibits calcification by strongly binding calcium ions to its Gla residues.[21] Significantly, calcification has been found to be prevalent in femoral atherosclerotic plaques of patients carrying a particular MGP allele, but this association does not apply for carotid plaques. This study demonstrates the use of B-mode US in locating calcification; however, this method does not allow for reliable quantitation of calcification because the image resolution does not allow for accurate delineation of plaque components (Table).

Intravascular ultrasound (IVUS) is an invasive method that details the relationship between plaque and vessel wall in real time throughout the coronary artery tree. The invasive nature of IVUS allows exact definition of not only the quantity but also the distribution of calcification within the vessel wall and the ability to classify different plaque substructures, helping to clarify ambiguous angiograms and delineate the exact nature of luminal encroachment. The central positioning of a high-frequency transducer within the target vessel facilitates high resolution of the arterial lumen-wall border, permitting a more precise definition of small ulcerations than is available by other diagnostic methods.[22] However, this method cannot be used routinely until the pathologic significance of plaque ulceration is clearly defined, thereby avoiding possible disturbance of an unstable plaque.[22] This method also enables identification of lesion subsets that may have an important natural history in development of atherosclerosis.[23,24] Four types of atherosclerotic plaque components can be distinguished using IVUS: (1) lipid-rich (hypoechoic), (2) fibromuscular (soft echoes), (3) fibrous (bright echoic), and (4) calcific (bright echoes with shadowing behind the lesion).[25] IVUS has been used to differentiate these components in several studies in vivo.[26] The precision and accuracy of calcification quantitation by IVUS is excellent.[27] In a study of calcium in culprit lesions after the placement of a stent, IVUS was used to assess the arc of calcium, which appears as a bright echogenic signal accompanied by an acoustic shadow in the arterial wall.[28] Calcium was quantified by 2 methods: (1) as the widest arc of calcium found in the stented segment, and (2) as the average arc of calcium in the proximal, middle, and distal sections of the stented segments. The results showed that calcium is less abundant in plaques associated with culprit stenoses and more abundant in plaques associated with stable angina.

Similarly, the calcium arc was used to quantify calcium in a study of coronary artery remodeling.[29] Overall, coronary arteries were observed to enlarge in most patients, with the exception of smokers. Also, no specific morphological features were found to be predictive of arterial remodeling. In another study focused on determining the relationship between smoking and calcification, the arc of calcium as determined by IVUS was applied to a regression equation that took into account age, gender, and smoking.[30] The results indicated that among patients with coronary artery disease, previous or current smokers have plaque areas with similar dimensions but less calcification than nonsmokers.

The method of measuring calcium content from IVUS images involves a process of gathering cross-sectional images at a reference site and at a plaque site to measure the arc of calcium.[31] These measurements take into account the amount of calcium versus the lumen surface size by converting the calcium arc to a percentage of the lumen surface, producing a more accurate measure of calcification.

US tissue characterization coupled with integrated backscatter (IB) analysis is effective in distinguishing lipidic, fibrotic, and calcific components in human atherosclerotic plaques.[32] This technique is capable of producing 2D images and IB images, the latter of which details biochemical and structural components of atherosclerotic lesions.[33] In conjunction with IVUS, IB data have been used to make color-coded maps of coronary arterial plaques according to 5 tissue components: lipid core with fibrous cap, intimal hyperplasia, fibrous tissue, calcification, and thrombus.[33,34]

The most commonly used method to identify or quantify calcification by US is IVUS (Table). However, combinations of US methods are also incorporated but are used primarily for visualization purposes, not quantifying calcification.[35–38] To determine the role of calcium–phosphate metabolism in cardiac valve calcification of hemodialysis patients, B-mode and Doppler US were used to image the areas of calcification and to determine the severity score of valvular calcifications

on the basis of thickness.[39] These scores were found to correlate with the calcium–phosphate product ([Ca]×[PO_4]) calculated from the serum concentrations of the individual atoms.

Electron Beam CT

CT is based on x-ray technology that computes axial images of the body. In standard CT scanning of the heart, multiple cross-sectional images are acquired from different angles. A 3D view of the heart is then created by compiling the axial images. Although CT renders high-resolution images of still objects, it is not fast enough to acquire such images of a beating heart; however, it does allow noninvasive detection and reproducible quantification of calcification in vivo (Table).

Electron beam CT (EBCT) has been used to determine the presence and amount of calcium accumulated in the coronary arteries. It is much faster than standard CT scanning, produces images in a fraction of a second, and acquires high-resolutions images of an artery even while the heart is beating. EBCT uses an electron beam in stationary tungsten targets, permitting very rapid scanning times.[40] Prospective electrocardiographic triggering is required for acquisition of images by EBCT to reduce cardiac motion artifacts. As a result, arterial fat and calcium accumulation can be visualized clearly by EBCT. In 100 milliseconds, serial transaxial images are obtained every 3 to 6 mm for purposes of detecting coronary artery calcium. Thinner sections have been found to provide more accurate results.[41,42] Current EBCT software permits quantification of calcium area and density. The images produced provide the basis for a patient's "calcium score," representing the total amount of calcium present in the artery and calculated using the following equation: calcium score=[sum of (suprathreshold area×N)]×T/3, in which N is a density index with a value of 1 to 4 based on a truncated peak CT number (a measure of density with a range of 130 to 499) and T is the slice thickness.[43] A calcium score of 0 indicates virtually no risk for a cardiac event; scores between 1 and 100 correlate with low risk for a cardiac event over the next 5 years; scores from 100 to 400 infer moderate risk for cardiac events; and scores >400 indicate high risk for a heart attack.[40] Although this cardiac risk classification is not scientifically validated, it is useful as a clinical method of diagnosis and prognosis of heart disease. Another system of quantifying calcification as analyzed by CT is the Agatston score, which can be calculated using the number, area, and peak Hounsfield numbers of the detected calcified lesions and is based on 3-mm slices acquired without overlap.[44] Volume and mass calculations also provide reproducible results. Additionally, percentiles of risk stratification have been suggested.[45]

EBCT provides an accurate, reliable alternative to the more commonly used stress tests but is more expensive than many comparable tests. Results of EBCT have been compared with those of 2D echocardiography,[46] Doppler US,[47] IVUS,[48] and angiography[48–50] and have been found to be highly accurate in localizing and quantifying calcifications in the heart. EBCT is also very effective for detecting stable calcification in the arterial wall, a feature highly correlated to age.[51]

An alternative method to EBCT is multidetector row spiral CT (MDCT) with electrocardiography gating.[52–56] MDCT allows image acquisition of thinner slices but requires higher radiation exposure. Quantification of calcification by MDCT is more accurate than by EBCT or IVUS. Noncalcified plaque can also be visualized by MDCT but requires the aid of injected contrast-enhancing dyes, and individual plaque components cannot be distinguished and quantified. Studies have been conducted to understand the differences in signal between stable and unstable angina[57,58] and within plaques to differentiate composition,[59] but CT is not yet a reliable source for quantifying calcification relative to other plaque components.

Magnetic Resonance Imaging

MRI is a powerful imaging technique that can produce images of anatomic structures and organs inside the body and often provides more spatial and contrast resolution than other imaging techniques such as CT, which requires x-ray images and the injection of a contrast dye. MRI is most effective at providing images of tissues or organs that contain water or lipid but is not as useful for imaging structures that contain rather low levels of these molecules, especially in the solid state. The sensitivity of in vivo images is enhanced by the use of phased array surface coils that can be placed near the anatomic site of interest.

MRI is capable of distinguishing various components of atherosclerotic plaques, such as fibrous tissue, lipids, calcification, and thrombus[60–62] (Figure 1A). This capability enables determining lesion type and monitoring the progression and regression of atherosclerotic plaques (Table). Calcification typically appears dark in standard T1-, T2-, and proton density–weighted (PDW) images (Figure 1A) and, hence, can be difficult to distinguish from the lumen of a black blood image (Figure 1C).

In a study of carotid artery calcification and white matter ischemia, calcification was graded using 2 methods: (1) extent of calcification based on degrees of the vessel circumference occupied by calcification, and (2) thickness of calcification.[63] In a study of the effects of lipid-lowering drugs on atherosclerotic plaques, the investigators used MRI to determine the calcium cluster area and its percentage of the total plaque area.[64] The other plaque components were quantified in the same way so that comparisons could be made. Patients treated with intensive lipid-altering therapy had significantly lower percentages of lipid and higher percentages of calcium than those who were untreated. However, changes in percentages of plaque components can be misleading because if the proportion of 1 component decreases (eg, lipid), then the proportion of the other components (eg, calcification) must necessarily increase if their masses do not change.

We are currently using MRI to quantify calcified atherosclerotic lesions in the superficial femoral artery. The resulting images are used to guide endovascular intervention such as stenting, bypass, or remote endarterectomy (J. Morrisett and A. Lumsden, unpublished results, 2005).

Ex Vivo Analysis

Whereas in vivo analysis of atherosclerotic plaques is useful for diagnosis and treatment, ex vivo analysis is instructive for

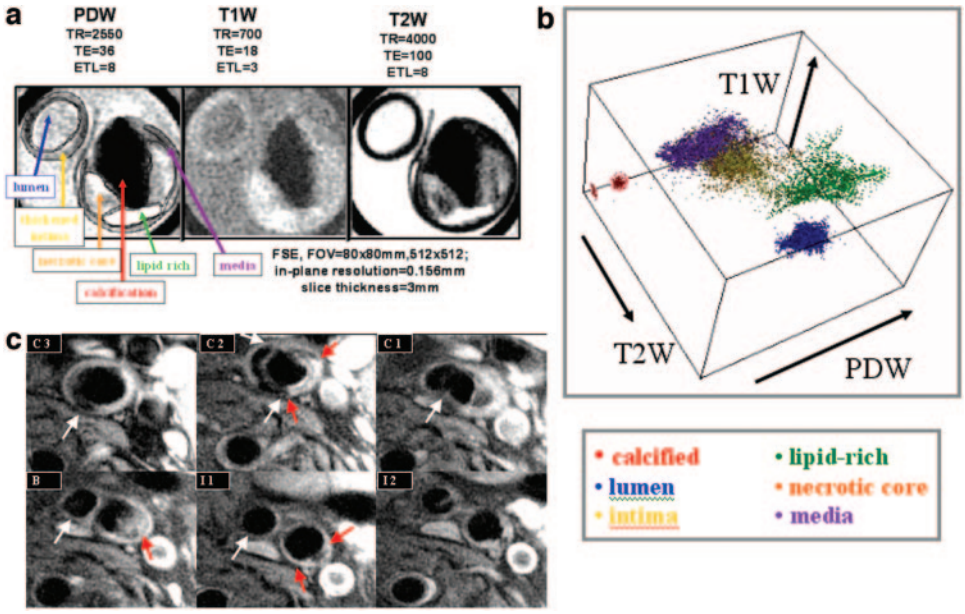

Figure 1. A, Three axial imaging sequences performed to generate different contrast weightings at each slice location: PDW, T1W, and T2W MR images of cadaveric arteries. Feature space analysis allows for quantitation of plaque components. TR indicates repetition time; TE, echo time; ETL, echo train length; FSE, fast spin-echo; FOV, field of view. B, Plotting intensities of pixels at the same *x-y* address in the T1W, T2W, and PDW images generates a feature space plot containing multiple clusters; each cluster corresponds to a component of the tissue: calcification, lumen, intima, lipid, necrotic core, and media. Each cluster was partially identified by imaging separate tissue components isolated by microdissection. Integration of the cluster volumes gives a quantitative measure of the corresponding component. (C. Karmonik and J. Morrisett, unpublished results, 2005). C, MRI axial slices (3 mm) of the left carotid artery of a 67-year-old woman presenting with >60% stenosis. The slices begin 9 mm below the bifurcation (C3) and extend 6 mm above it into the internal branch (I2). The compositional heterogeneity of the vessel wall and partially occluded lumen is evident. Slice C3 has a patent lumen, but disease of the wall is apparent from the darker area (calcification) at 7:00 (white arrow). This feature becomes more prominent in slice C2, extending from 6:00 to 12:00 (white arrows); concentric bright bands (fibrous cap and lipid core) are seen from 2:00 to 6:00 (red arrows). Slice C1 contains an indentation indicating the beginning of the flow divider (white arrow); the beginning of the orifice of the partially occluded internal branch is evident. Slice B cuts directly through the bifurcation, clearly showing a rather patent external carotid (white arrow) but a highly stenosed internal carotid (red arrow); the occluding plaque exhibits intermediate brightness typical of lipid rich lesions. Slice I1 shows complete separation of the 2 branches; the external carotid (white arrow) has virtually no disease, whereas the internal carotid shows significant wall thickening at 4:00 to 7:00 (red arrows). The spatial and contrast resolution of these representative images are essential for the separation and quantification of plaque components.

understanding mechanisms of plaque formation and establishing the identity of features of plaque images obtained in vivo. Ex vivo studies have been performed on CCA and CEA tissues. Carotid arteries from human cadavers provide anatomic information about the medial and adventitial layers, which are not usually present in CEA tissues. This advantage is diminished partly by the alteration in CCA tissue structure because of formalin fixation, in contrast to CEA tissue, which is obtained fresh or stored in a cryoprotecting buffer at −20°C without loss of structure

Micro-CT

Micro-CT (μCT) is similar to CT in that x-ray images are acquired at multiple angles around the object followed by computation of its tomogram. Currently available μCT instrumentation is typically a compact, desktop x-ray system for nondestructive reconstruction of 3D tissue microstructure with high spatial resolution. With μCT, it is possible to: (1) obtain transmission shadow images of tissue; (2) reconstruct any cross-section of the complete 3D object microstructure; (3) calculate distance, surface area, and volume; (4) analyze density and porosity of an object; and (5) achieve 3D rendering and realistic visualization through animation of the reconstructed images (Table).

With μCT, 3D radioscopic image data are acquired rapidly and noninvasively to capture thin cross-sections. Because of the low-dose radiation used, mice and rats can be imaged serially by this method. The resulting data, which have spatial resolution of 20 μm, are used in reconstruction calculations to generate realistic 3D images and to calculate morphological parameters. A major application of μCT has been to quantify the 3D microstructure of bone and to provide quantitative information about its functionality, porosity, and mineral density, making the technique useful for early detection of various bone pathologies, including osteoporosis.[65–68]

μCT can also be used to study calcification of the arterial wall[68,69] and enables nondestructive visualization and localization of CHA in very thin tissue slices, although it does not allow for delineation of other plaque components (Figure 2). Two morphological distributions are observed: (1) calcification nodules localized mainly in the necrotic core or luminal surface, and (2) calcification plates localized more to the medial layer, often extending around a substantial fraction of its circumference. Calibrating the μCT system with known amounts of CHA is done by scanning a 96-well microtiter plate having wells

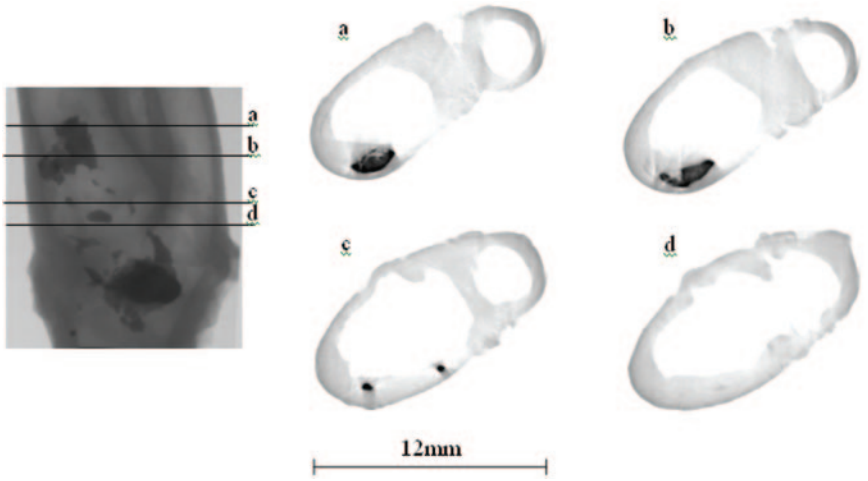

Figure 2. μCT images of a CCA. Axial slice images (0.3 mm) reveal a large calcification plate (a and b) and small nodules (c) in the internal carotid but no calcification in the common carotid (d).

filled with different amounts of hydrated CHA. The sum of electron dense areas in successive slices of CHA in each well enables construction of a standard calibration curve that can be used for calculation of unknown samples.

Magnetic Resonance Imaging

Ex vivo samples can be imaged by MRI using coils of different geometries. A solenoid coil (30-mm diameter) is convenient for imaging single samples at very high resolution. A phased array coil (6-cm width) is convenient for multiple samples at high resolution. MRI analysis of CEA specimens can be performed using the same sample holder but smaller sample tubes than used for CCA imaging.

Representative magnetic resonance (MR) images of CEA tissues are shown in Figure 1. Plaque components, including collagenous cap, necrotic core, hemorrhage, and calcification can be distinguished in MR images of plaques.[70–72] These components can also be mapped according to their contrast weightings, which allow for integration of the components and quantification. Multicontrast-weighted MR images of carotid plaques have also been used to develop classification maps useful in distinguishing plaque components more effectively[69] (Table).

In a study of left and right CCA, MRI and EBCT were used to determine arterial wall volume and calcification score.[73] The results indicated that total wall volume and plaque calcification burden were similar for the left and right arteries, suggesting that atherosclerosis is a bilaterally symmetrical disease.

In PDW images of CEA tissues, regions of calcification appear dark (Figure 3b). When these tissues are embedded in paraffin, the calcified regions appear white (Figure 3a). Integration of the calcified regions visualized by each method provided 2 sets of integrated areas (MRI and embedded tissue imaging) that were highly correlated (R^2=0.99; Figure 3c).

Three-D images have been obtained of human CCA using multicontrast-weighted fast spin-echo imaging.[74] A cluster analysis technique called spatially enhanced cluster analysis objectively classified and quantified multicontrast MR images. The cluster technique divides data into groups with strong associations by iteratively minimizing a characteristic of the cluster. Using this technique, plaque components such as calcification can be differentiated by color and then quantified.

^{31}P MR Spectroscopy

MR spectroscopy (MRS) is useful for quantifying nuclei in specific magnetic environments and has been used extensively to study biomolecules in isotropic solutions. Magic

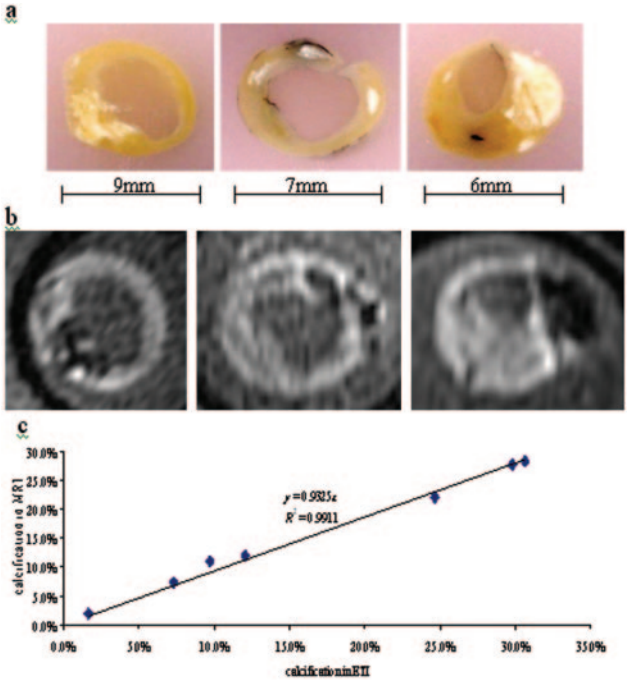

Figure 3. a, A CEA specimen was microdissected into segments ≈1.0 cm in length. Selected segments were fixed and embedded in paraffin by conventional methods. From each block, excess paraffin was lifted with a microtome until a full artery cross-section was exposed. The fixed tissue cross-sections were digitally photographed and contrast-manually enhanced with the NIH image analysis program ImageJ 1.30v. b, Each digital image was matched using eFilm Workstation 1.8.3 with the MRI image of the closest morphology. For each image, the total artery area, total lumen area, and total calcified area were circumscribed independently using freehand area selection in ImageJ and measured by automated integration. Percent calcification was then calculated for each image. c, Comparison of percent calcification in CEA specimens detected by MRI (b) and embedded tissue imaging (ETI; a; S. Marvel and J. Morrisett, unpublished results, 2005).

angle spinning (MAS) extends the power of MRS to include determining chemical and structural properties of anisotropic liquid crystalline and solid samples. The mineral content of bone can be quantified using ^{31}P MRS because the phosphate of CHA is distinguishable from P_i, from phosphorylated metabolites dissolved in the cytosol, and from the polar head groups of phospholipids in membranes.[75,76] Accordingly, ^{31}P MAS MRS can be used for rapid quantification of CHA in atherosclerotic plaques.[77,78]

In a study of lipid phases and CHA deposits in human atherosclerotic lesions, a plaque with low lipid content (weak ^{13}C MAS MRS signals) and extensive calcification (strong ^{31}P MAS MRS signals) has been used to determine CHA content.[77] After delipidation of the plaque, the ^{31}P MAS MRS signal intensity showed no change, indicating that the ^{31}P signal resulted from nonlipid phosphorus. Based on the intensity of the ^{31}P MAS MRS peak, the phosphorus content could be calculated, followed by stoichiometric conversion to CHA content.

The integrated ^{31}P signal intensity in plaques can be calibrated using synthetic CHA and chicken bone powder as reference compounds.[78] Comparisons of ^{31}P peak intensities showed that the chicken bone powder provided the best calibration, presumably because the synthetic CHA has a more ordered crystalline structure than the biological samples. This technique is somewhat destructive because delipidation leaves the tissue in a non-native state. ^{31}P MAS MRS is generally restricted to ex vivo samples <1 cm^3 (Table).

Tissue Digital Photography

Digital photographs of CEA specimens are useful for documenting tissue features lost during processing (eg, thrombus and calcification) for microscopy and can capture subtle textural and morphological features not detected by other techniques (Figure 4). Although differences in photographic color are useful for qualitatively distinguishing between calcified and lipid-rich regions, the contrast is not sufficient to accurately quantify the 2 types of plaque components. However, estimating calcium in these tissues becomes feasible when they are embedded in paraffin and digitally photographed (Figure 3). The total artery area, total lumen area, and total calcified area can be integrated and these areas used to calculate the percent calcification for each image. Although paraffin-thin sections frequently lose some of the calcified component during cutting, the remaining block has a smooth surface that facilitates quantitation (Table).

Histology

Conventional histology is used widely to analyze the structure of animal and plant tissues. Fixed and stained CEA specimens viewed by light microscopy are useful for identifying plaque components.[79] For calcified tissues in paraffin blocks, cutting intact cross-sections can be difficult. Exemplary images from histological analysis are shown in Figure 5. Cutting calcification in frozen sections is even more challenging, usually requiring at least treatment with nitric acid or EDTA. However, these treatments cause calcium depletion and can reduce immunoreactivity of calcium-binding proteins. The percentages of calcification and other plaque components can be determined by area integration.[80,81]

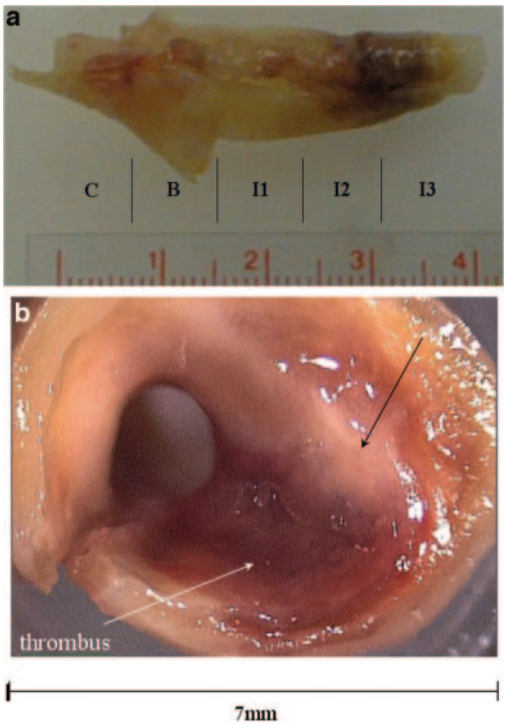

Figure 4. Digital photograph of a fresh CEA specimen (a) illustrating the presence of extensive calcification and thrombus in segment I3 (b). Thrombus appears as a dark red area, and calcification appears as a white–pink area. The shiny white areas are optical artifacts.

Embedding tissue in plastic helps prevent loss of calcification during sectioning while retaining stain and antibody reactivity. Representative plastic embedded thin sections are shown in Figure 6. Paraffin blocks and frozen sections are attended by significant loss of calcification; however, the time-consuming process of tissue embedding in plastic allows retention of calcification and its quantification (Table).

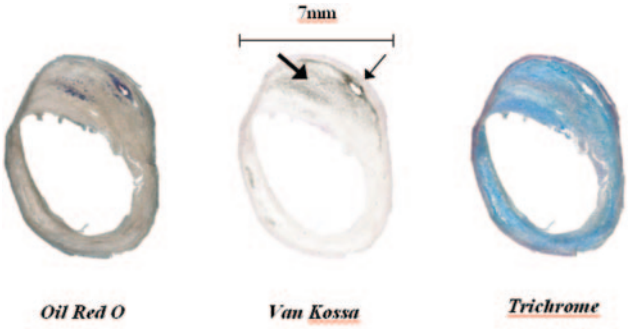

Figure 5. From the internal branch of the left carotid artery, fibro-fatty lesions have been segmented and fixed in paraffin blocks. Then 10-μm histology sections prepared from original blocks were stained with: a, Oil Red O, to stain lipid purple, and nuclei brown; b, Van Kossa, to stain calcium salts black, nuclei red, and cytoplasm light pink; and c, trichrome, to stain muscle fibers red, collagen blue, and nuclei blue to black. These sections illustrate distribution of small calcification nodules through the midintimal area (heavy arrow) and loss of calcification from a deep-intimal area near 2:00 (light arrow).

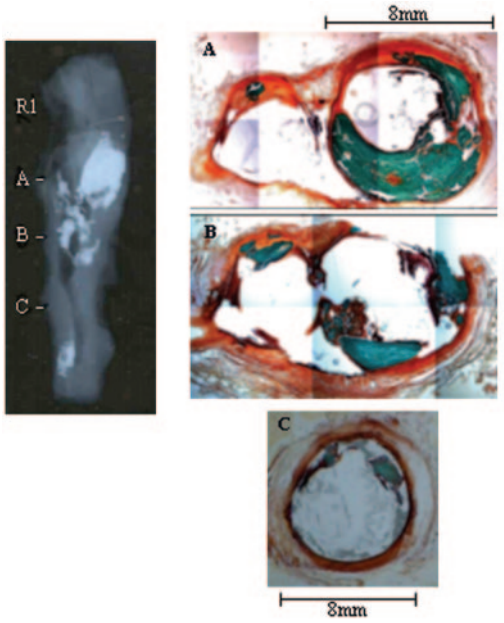

Figure 6. X-ray image and corresponding thin-section light micrographs from right CCA fixed in 10% formalin. After fixation, the CEA samples are dehydrated in a graded series of ethanol washes and embedded in glycomethylmethacrylate. After polymerization, thin sections (10 to 30 um) are prepared using the Exakt System modified sawing microtome technique.[84] Sections are stained with a Modified Goldner Tri-Chrome reagent for plastic sections for which calcification appears blue–green.

Chemical Analysis

Atomic absorption spectroscopy (AAS) is a sensitive analytical technique used to determine the concentration of metals in liquid samples. In their elemental form, metals absorb ultraviolet light when excited by heat, and each metal has a characteristic wavelength that will be absorbed. The amount of light absorbed is proportional to the concentration of the element in the solution. Measurements are made separately for each element of interest. The method is very sensitive and can measure trace elements down to the parts per million level. Because calcium is one of the metals detectable by AAS, this method is useful in determining calcium concentration in CEA samples. Stoichiometry can be used to calculate the quantity of CHA in the samples (Table).

Another method for chemically analyzing CHA in CEA samples uses the phosphomolybdate reagent, which quantifies the amount of elemental phosphorus in a sample.[82] The sample is digested in sulfuric acid and oxidized with hydrogen peroxide to liberate elemental phosphorus. Ammonium molybdate and 1-amino-2-naphthol-4-sulfonic acid are added to produce a solution that absorbs at 830 nm. The concentration of phosphorus is determined from a calibration curve of various concentrations of a standard phosphate salt. The stoichiometry of CHA, $Ca_{10}(PO_4)_6(OH)_2$, can be used to convert the measured phosphorus concentration to CHA mass. A useful alternative method uses o-cresolphthalein for calcium determination.[83] Fura and Indo ratiometric calcium indicators are excited with UV light, allowing for quantification of calcium content as well.[84]

Concluding Comments

Selecting an appropriate method of calcification quantification depends on the nature of the specimen and the desired results (Table). Although the in vivo methods of US, EBCT, and MRI are all capable of differentiating plaque components, IVUS and MRI have the highest spatial resolution. In ex vivo analyses, μCT and MRI are the principal methods for visualizing calcified thin slices and creating 3D reconstruction of the specimen. Digital photography is useful for capturing a visual record of intact tissues and tissue fragments before processing by embedding or homogenization. Histological sections provide morphological information that is currently the gold reference standard for validating many imaging techniques. ^{31}P MAS MRS and the microphosphorus chemical assay for calcification quantification rely on chemical stoichiometry to convert the concentration of phosphorus atoms to CHA. The chemical assay is more amenable to high throughput but requires sample destruction. AAS is probably the most sensitive method for calcium quantification; it has the same capabilities and limitations as those of the microphosphorus assay. These qualitative and quantitative methods will likely see increasing use in future investigations of vascular calcification.

Acknowledgments

This work was supported in part by the National Institutes of Health grants HL63090 and HL07812. The authors thank Catherine Ambrose, PhD, and Tiffany Sheffield of the Bone Histomorphometry and Biomaterials Laboratory in the Department of Orthopaedic Surgery at the University of Texas-Houston Medical School for the plastic embedded histochemical preparations.

References

1. Alberts B. *Molecular Biology of the Cell.* 4th ed. New York, NY: Garland Science; 2002.
2. Vattikuti R, Towler DA. Osteogenic regulation of vascular calcification: an early perspective. *Am J Physiol Endocrinol Metab*. 2004;286: E686–E696.
3. Heino TJ, Hentunen TA, Vaananen HK. Osteocytes inhibit osteoclastic bone resorption through transforming growth factor-beta: enhancement by estrogen. *J Cell Biochem*. 2002;85:185–197.
4. Becker GL. Calcification mechanisms: roles for cells and mineral. *J Oral Pathol.* 1977;6:307–315.
5. Trion A, van der Laarse A. Vascular smooth muscle cells and calcification in atherosclerosis. *Am Heart J.* 2004;147:808–814.
6. Wu LN, Ishikawa Y, Sauer GR, Genge BR, Mwale F, Mishima H, Wuthier RE. Morphological and biochemical characterization of mineralizing primary cultures of avian growth plate chondrocytes: evidence for cellular processing of Ca2+ and Pi prior to matrix mineralization. *J Cell Biochem*. 1995;57:218–237.
7. Eanes ED, Gillessen IH, Posner AS. Intermediate states in the precipitation of hydroxyapatite. *Nature.* 1965;208:365–367.
8. Seuwen K, Boddeke HG, Migliaccio S, Perez M, Taranta A, Teti A. A novel calcium sensor stimulating inositol phosphate formation and [Ca2+]i signaling expressed by GCT23 osteoclast-like cells. *Proc Assoc Am Physicians*. 1999;111:70–81.
9. Wenisch S, Stahl JP, Horas U, Heiss C, Kilian O, Trinkaus K, Hild A, Schnettler R. In vivo mechanisms of hydroxyapatite ceramic degradation by osteoclasts: fine structural microscopy. *J Biomed Mater Res A*. 2003; 67:713–718.
10. Mostov K, Werb Z. Journey across the osteoclast. *Science.* 1997;276: 219–220.
11. Doherty TM, Asotra K, Fitzpatrick LA, Qiao JH, Wilkin DJ, Detrano RC, Dunstan CR, Shah PK, Rajavashisth TB. Calcification in atherosclerosis: bone biology and chronic inflammation at the arterial crossroads. *Proc Natl Acad Sci U S A*. 2003;100:11201–11206.

12. Tintut Y, Demer LL. Recent advances in multifactorial regulation of vascular calcification. *Curr Opin Lipidol*. 2001;12:555–560.
13. Parhami F, Morrow AD, Balucan J, Leitinger N, Watson AD, Tintut Y, Berliner JA, Demer LL. Lipid oxidation products have opposite effects on calcifying vascular cell and bone cell differentiation. A possible explanation for the paradox of arterial calcification in osteoporotic patients. *Arterioscler Thromb Vasc Biol*. 1997;17:680–687.
14. Kiechl S, Schett G, Wenning G, Redlich K, Oberhollenzer M, Mayr A, Santer P, Smolen J, Poewe W, Willeit J. Osteoprotegerin is a risk factor for progressive atherosclerosis and cardiovascular disease. *Circulation*. 2004;109:2175–2180.
15. Golledge J, McCann M, Mangan S, Lam A, Karan M. Osteoprotegerin and osteopontin are expressed at high concentrations within symptomatic carotid atherosclerosis. *Stroke*. 2004;35:1636–1641.
16. Gronholdt ML. Ultrasound and lipoproteins as predictors of lipid-rich, rupture-prone plaques in the carotid artery. *Arterioscler Thromb Vasc Biol*. 1999;19:2–13.
17. Barry R, Pienaar C, Nel CJ. Accuracy of B-mode ultrasonography in detecting carotid plaque hemorrhage and ulceration. *Ann Vasc Surg*. 1990;4:466–470.
18. Schreiner PJ, Heiss G, Tyroler HA, Morrisett JD, Davis CE, Smith R. Race and gender differences in the association of Lp(a) with carotid artery wall thickness. The Atherosclerosis Risk in Communities (ARIC) Study. *Arterioscler Thromb Vasc Biol*. 1996;16:471–478.
19. de Groot E, Jukema JW, Montauban van Swijndregt AD, Zwinderman AH, Ackerstaff RG, van der Steen AF, Bom N, Lie KI, Bruschke AV. B-mode ultrasound assessment of pravastatin treatment effect on carotid and femoral artery walls and its correlations with coronary arteriographic findings: a report of the Regression Growth Evaluation Statin Study (REGRESS). *J Am Coll Cardiol*. 1998;31:1561–1567.
20. Wagenknecht LE, Langefeld CD, Carr JJ, Riley W, Freedman BI, Moossavi S, Bowden DW. Race-specific relationships between coronary and carotid artery calcification and carotid intimal medial thickness. *Stroke*. 2004;35:e97–e99.
21. Herrmann SM, Whatling C, Brand E, Nicaud V, Gariepy J, Simon A, Evans A, Ruidavets JB, Arveiler D, Luc G, Tiret L, Henney A, Cambien F. Polymorphisms of the human matrix Gla protein (MGP) gene, vascular calcification, myocardial infarction. *Arterioscler Thromb Vasc Biol*. 2000;20:2386–2393.
22. Miskolczi L, Guterman LR, Flaherty JD, Hopkins LN. Depiction of carotid plaque ulceration and other plaque-related disorders by intravascular sonography: a flow chamber study. *Am J Neuroradiol*. 1996;17:1881–1890.
23. Maehara A, Fitzgerald PJ. Coronary calcification: assessment by intravascular ultrasound imaging. *Z Kardiol*. 2000;89(suppl 2):112–116.
24. Tobis JM, Mallery J, Mahon D, Lehmann K, Zalesky P, Griffith J, Gessert J, Moriuchi M, McRae M, Dwyer ML, et al. Intravascular ultrasound imaging of human coronary arteries in vivo. Analysis of tissue characterizations with comparison to in vitro histological specimens. *Circulation*. 1991;83:913–926.
25. Gussenhoven EJ, Essed CE, Frietman P, van Egmond F, Lancee CT, van Kappellen WH, Roelandt J, Serruys PW, Gerritsen GP, van Urk H, et al. Intravascular ultrasonic imaging: histologic and echographic correlation. *Eur J Vasc Surg*. 1989;3:571–576.
26. Chiesa G, Di Mario C, Colombo N, Vignati L, Marchesi M, Monteggia E, Parolini C, Lorenzon P, Laucello M, Lorusso V, Adamian M, Franceschini G, Newton R, Sirtori CR. Development of a lipid-rich, soft plaque in rabbits, monitored by histology and intravascular ultrasound. *Atherosclerosis*. 2001;156:277–287.
27. Palmer ND, Northridge D, Lessells A, McDicken WN, Fox KA. In vitro analysis of coronary atheromatous lesions by intravascular ultrasound; reproducibility and histological correlation of lesion morphology. *Eur Heart J*. 1999;20:1701–1706.
28. Beckman JA, Ganz J, Creager MA, Ganz P, Kinlay S. Relationship of clinical presentation and calcification of culprit coronary artery stenoses. *Arterioscler Thromb Vasc Biol*. 2001;21:1618–1622.
29. Weissman NJ, Sheris SJ, Chari R, Mendelsohn FO, Anderson WD, Breall JA, Tanguay JF, Diver DJ. Intravascular ultrasonic analysis of plaque characteristics associated with coronary artery remodeling. *Am J Cardiol*. 1999;84:37–40.
30. Kornowski R. Impact of smoking on coronary atherosclerosis and remodeling as determined by intravascular ultrasonic imaging. *Am J Cardiol*. 1999;83:443–445, A449.
31. Scott DS, Arora UK, Farb A, Virmani R, Weissman NJ. Pathologic validation of a new method to quantify coronary calcific deposits in vivo using intravascular ultrasound. *Am J Cardiol*. 2000;85:37–40.
32. Urbani MP, Picano E, Parenti G, Mazzarisi A, Fiori L, Paterni M, Pelosi G, Landini L. In vivo radiofrequency-based ultrasonic tissue characterization of the atherosclerotic plaque. *Stroke*. 1993;24:1507–1512.
33. Kawasaki M, Takatsu H, Noda T, Ito Y, Kunishima A, Arai M, Nishigaki K, Takemura G, Morita N, Minatoguchi S, Fujiwara H. Noninvasive quantitative tissue characterization and two-dimensional color-coded map of human atherosclerotic lesions using ultrasound integrated backscatter: comparison between histology and integrated backscatter images. *J Am Coll Cardiol*. 2001;38:486–492.
34. Kawasaki M, Takatsu H, Noda T, Sano K, Ito Y, Hayakawa K, Tsuchiya K, Arai M, Nishigaki K, Takemura G, Minatoguchi S, Fujiwara T, Fujiwara H. In vivo quantitative tissue characterization of human coronary arterial plaques by use of integrated backscatter intravascular ultrasound and comparison with angioscopic findings. *Circulation*. 2002;105:2487–2492.
35. Brandt T, Knauth M, Wildermuth S, Winter R, von Kummer R, Sartor K, Hacke W. CT angiography and Doppler sonography for emergency assessment in acute basilar artery ischemia. *Stroke*. 1999;30:606–612.
36. London GM, Guerin AP, Marchais SJ, Metivier F, Pannier B, Adda H. Arterial media calcification in end-stage renal disease: impact on all-cause and cardiovascular mortality. *Nephrol Dial Transplant*. 2003;18:1731–1740.
37. Pai SS, Bude RO. Sonographic appearance of extensive hepatic arterial calcification mimicking pneumobilia. *J Clin Ultrasound*. 2002;30:38–41.
38. Whitehall J, Smith M, Altamirano L. Idiopathic infantile arterial calcification: sonographic findings. *J Clin Ultrasound*. 2003;31:497–501.
39. Ribeiro S, Ramos A, Brandao A, Rebelo JR, Guerra A, Resina C, Vila-Lobos A, Carvalho F, Remedio F, Ribeiro F. Cardiac valve calcification in haemodialysis patients: role of calcium-phosphate metabolism. *Nephrol Dial Transplant*. 1998;13:2037–2040.
40. O'Rourke RA, Brundage BH, Froelicher VF, Greenland P, Grundy SM, Hachamovitch R, Pohost GM, Shaw LJ, Weintraub WS, Winters WL Jr, Forrester JS, Douglas PS, Faxon DP, Fisher JD, Gregoratos G, Hochman JS, Hutter AM Jr, Kaul S, Wolk MJ. American College of Cardiology/American Heart Association Expert Consensus document on electron-beam computed tomography for the diagnosis and prognosis of coronary artery disease. *Circulation*. 2000;102:126–140.
41. Vliegenthart R, Song B, Hofman A, Witteman JC, Oudkerk M. Coronary calcification at electron-beam CT: effect of section thickness on calcium scoring in vitro and in vivo. *Radiology*. 2003;229:520–525.
42. Callister T, Janowitz W, Raggi P. Sensitivity of two electron beam tomography protocols for the detection and quantification of coronary artery calcium. *Am J Roentgenol*. 2000;175:1743–1746.
43. Watson KE, Abrolat ML, Malone LL, Hoeg JM, Doherty T, Detrano R, Demer LL. Active serum vitamin D levels are inversely correlated with coronary calcification. *Circulation*. 1997;96:1755–1760.
44. Agatston AS, Janowitz WR, Hildner FJ, Zusmer NR, Viamonte M Jr, Detrano R. Quantification of coronary artery calcium using ultrafast computed tomography. *J Am Coll Cardiol*. 1990;15:827–832.
45. Raggi P, James G. Coronary calcium screening and coronary risk stratification. *Curr Atheroscler Rep*. 2004;6:107–111.
46. Walsh CR, Larson MG, Kupka MJ, Levy D, Vasan RS, Benjamin EJ, Manning WJ, Clouse ME, O'Donnell CJ. Association of aortic valve calcium detected by electron beam computed tomography with echocardiographic aortic valve disease and with calcium deposits in the coronary arteries and thoracic aorta. *Am J Cardiol*. 2004;93:421–425.
47. Messika-Zeitoun D, Aubry MC, Detaint D, Bielak LF, Peyser PA, Sheedy PF, Turner ST, Breen JF, Scott C, Tajik AJ, Enriquez-Sarano M. Evaluation and clinical implications of aortic valve calcification measured by electron-beam computed tomography. *Circulation*. 2004;110:356–362.
48. Baumgart D, Schmermund A, Goerge G, Haude M, Ge J, Adamzik M, Sehnert C, Altmaier K, Groenemeyer D, Seibel R, Erbel R. Comparison of electron beam computed tomography with intracoronary ultrasound and coronary angiography for detection of coronary atherosclerosis. *J Am Coll Cardiol*. 1997;30:57–64.
49. Woodcock RJ Jr, Goldstein JH, Kallmes DF, Cloft HJ, Phillips CD. Angiographic correlation of CT calcification in the carotid siphon. *Am J Neuroradiol*. 1999;20:495–499.
50. Budoff MJ, Diamond GA, Raggi P, Arad Y, Guerci AD, Callister TQ, Berman D. Continuous probabilistic prediction of angiographically significant coronary artery disease using electron beam tomography. *Circulation*. 2002;105:1791–1796.

51. Pirich C, Leber A, Knez A, Bengel FM, Nekolla SG, Haberl R, Schwaiger M. Relation of coronary vasoreactivity and coronary calcification in asymptomatic subjects with a family history of premature coronary artery disease. *Eur J Nucl Med Mol Imaging*. 2004;31:663–670.
52. Achenbach S, Ropers D, Hoffmann U, MacNeill B, Baum U, Pohle K, Brady TJ, Pomerantsev E, Ludwig J, Flachskampf FA, Wicky S, Jang IK, Daniel WG. Assessment of coronary remodeling in stenotic and nonstenotic coronary atherosclerotic lesions by multidetector spiral computed tomography. *J Am Coll Cardiol*. 2004;43:842–847.
53. Achenbach S, Ropers D, Pohle K, Anders K, Baum U, Hoffmann U, Moselewski F, Ferencik M, Brady TJ. Clinical results of minimally invasive coronary angiography using computed tomography. *Cardiol Clin*. 2003;21:549–559.
54. Achenbach S, Hoffmann U, Ferencik M, Wicky S, Brady TJ. Tomographic coronary angiography by EBCT and MDCT. *Prog Cardiovasc Dis*. 2003;46:185–195.
55. Achenbach S, Daniel WG. Imaging of coronary atherosclerosis using computed tomography: current status and future directions. *Curr Atheroscler Rep*. 2004;6:213–218.
56. Schroeder S, Kuettner A, Kopp AF, Heuschmidt M, Burgstahler C, Herdeg C, Claussen CD. Noninvasive evaluation of the prevalence of noncalcified atherosclerotic plaques by multi-slice detector computed tomography: results of a pilot study. *Int J Cardiol*. 2003;92:151–155.
57. Leber AW, Knez A, Mukherjee R, White C, Huber A, Becker A, Becker CR, Reiser M, Haberl R, Steinbeck G. Usefulness of calcium scoring using electron beam computed tomography and noninvasive coronary angiography in patients with suspected coronary artery disease. *Am J Cardiol*. 2001;88:219–223.
58. Leber AW, Knez A, White CW, Becker A, von Ziegler F, Muehling O, Becker C, Reiser M, Steinbeck G, Boekstegers P. Composition of coronary atherosclerotic plaques in patients with acute myocardial infarction and stable angina pectoris determined by contrast-enhanced multislice computed tomography. *Am J Cardiol*. 2003;91:714–718.
59. Leber AW, Knez A, Becker A, Becker C, von Ziegler F, Nikolaou K, Rist C, Reiser M, White C, Steinbeck G, Boekstegers P. Accuracy of multidetector spiral computed tomography in identifying and differentiating the composition of coronary atherosclerotic plaques: a comparative study with intracoronary ultrasound. *J Am Coll Cardiol*. 2004;43:1241–1247.
60. Cai JM, Hatsukami TS, Ferguson MS, Small R, Polissar NL, Yuan C. Classification of human carotid atherosclerotic lesions with in vivo multicontrast magnetic resonance imaging. *Circulation*. 2002;106:1368–1373.
61. Cappendijk VC, Cleutjens KB, Heeneman S, Schurink GW, Welten RJ, Kessels AG, van Suylen RJ, Daemen MJ, van Engelshoven JM, Kooi ME. In vivo detection of hemorrhage in human atherosclerotic plaques with magnetic resonance imaging. *J Magn Reson Imaging*. 2004;20:105–110.
62. Correia LC, Atalar E, Kelemen MD, Ocali O, Hutchins GM, Fleg JL, Gerstenblith G, Zerhouni EA, Lima JA. Intravascular magnetic resonance imaging of aortic atherosclerotic plaque composition. *Arterioscler Thromb Vasc Biol*. 1997;17:3626–3632.
63. Babiarz LS, Yousem DM, Wasserman BA, Wu C, Bilker W, Beauchamp NJ Jr. Cavernous carotid artery calcification and white matter ischemia. *Am J Neuroradiol*. 2003;24:872–877.
64. Zhao XQ, Yuan C, Hatsukami TS, Frechette EH, Kang XJ, Maravilla KR, Brown BG. Effects of prolonged intensive lipid-lowering therapy on the characteristics of carotid atherosclerotic plaques in vivo by MRI: a case-control study. *Arterioscler Thromb Vasc Biol*. 2001;21:1623–1629.
65. Anderson HC, Sipe JB, Hessle L, Dhanyamraju R, Atti E, Camacho NP, Millan JL. Impaired calcification around matrix vesicles of growth plate and bone in alkaline phosphatase-deficient mice. *Am J Pathol*. 2004;164:841–847.
66. Doschak MR, Cooper DM, Huculak CN, Matyas JR, Hart DA, Hallgrimsson B, Zernicke RF, Bray RC. Angiogenesis in the distal femoral chondroepiphysis of the rabbit during development of the secondary centre of ossification. *J Anat*. 2003;203:223–233.
67. Verna C, Dalstra M, Wikesjo UM, Trombelli L. Healing patterns in calvarial bone defects following guided bone regeneration in rats. A micro-CT scan analysis. *J Clin Periodontol*. 2002;29:865–870.
68. Ritman EL, Bolander ME, Fitzpatrick LA, Turner RT. Micro-CT imaging of structure-to-function relationship of bone microstructure and associated vascular involvement. *Technol Health Care*. 1998;6:403–412.
69. Clarke SE, Hammond RR, Mitchell JR, Rutt BK. Quantitative assessment of carotid plaque composition using multicontrast MRI and registered histology. *Magn Reson Med*. 2003;50:1199–1208.
70. Coombs BD, Rapp JH, Ursell PC, Reilly LM, Saloner D. Structure of plaque at carotid bifurcation: high-resolution MRI with histological correlation. *Stroke*. 2001;32:2516–2521.
71. Shinnar M, Fallon JT, Wehrli S, Levin M, Dalmacy D, Fayad ZA, Badimon JJ, Harrington M, Harrington E, Fuster V. The diagnostic accuracy of ex vivo MRI for human atherosclerotic plaque characterization. *Arterioscler Thromb Vasc Biol*. 1999;19:2756–2761.
72. Morrisett J, Vick W, Sharma R, Lawrie G, Reardon M, Ezell E, Schwartz J, Hunter G, Gorenstein D. Discrimination of components in atherosclerotic plaques from human carotid endarterectomy specimens by magnetic resonance imaging ex vivo. *Magn Reson Imaging*. 2003;21:465–474.
73. Adams GJ, Simoni DM, Bordelon CB Jr, Vick GW III, Kimball KT, Insull W Jr, Morrisett JD. Bilateral symmetry of human carotid artery atherosclerosis. *Stroke*. 2002;33:2575–2580.
74. Itskovich VV, Samber DD, Mani V, Aguinaldo JG, Fallon JT, Tang CY, Fuster V, Fayad ZA. Quantification of human atherosclerotic plaques using spatially enhanced cluster analysis of multicontrast-weighted magnetic resonance images. *Magn Reson Med*. 2004;52:515–523.
75. Brown CE, Allaway JR, Brown KL, Battocletti JH. Noninvasive evaluation of mineral content of bone without use of ionizing radiation. *Clin Chem*. 1987;33:227–236.
76. Hsieh MF, Perng LH, Chin TS, Perng HG. Phase purity of sol-gel-derived hydroxyapatite ceramic. *Biomaterials*. 2001;22:2601–2607.
77. Guo W, Morrisett JD, Lawrie GM, DeBakey ME, Hamilton JA. Identification of different lipid phases and calcium phosphate deposits in human carotid artery plaques by MAS NMR spectroscopy. *Magn Reson Med*. 1998;39:184–189.
78. Guo W, Morrisett JD, DeBakey ME, Lawrie GM, Hamilton JA. Quantification in situ of crystalline cholesterol and calcium phosphate hydroxyapatite in human atherosclerotic plaques by solid-state magic angle spinning NMR. *Arterioscler Thromb Vasc Biol*. 2000;20:1630–1636.
79. Denzel C, Lell M, Maak M, Hockl M, Balzer K, Muller KM, Fellner C, Fellner FA, Lang W. Carotid artery calcium: accuracy of a calcium score by computed tomography-an in vitro study with comparison to sonography and histology. *Eur J Vasc Endovasc Surg*. 2004;28:214–220.
80. Schulte-Altedorneburg G, Droste DW, Haas N, Kemeny V, Nabavi DG, Fuzesi L, Ringelstein EB. Preoperative B-mode ultrasound plaque appearance compared with carotid endarterectomy specimen histology. *Acta Neurol Scand*. 2000;101:188–194.
81. Bassiouny HS, Davis H, Massawa N, Gewertz BL, Glagov S, Zarins CK. Critical carotid stenoses: morphologic and chemical similarity between symptomatic and asymptomatic plaques. *J Vasc Surg*. 1989;9:202–212.
82. Bartlett GR. Phosphorus assay in column chromatography. *J Biol Chem*. 1959;234:466–468.
83. Fischer JW, Steitz SA, Johnson PY, Burke A, Kolodgie F, Virmani R, Giachelli C, Wight TN. Decorin promotes aortic smooth muscle cell calcification and colocalizes to calcified regions in human atherosclerotic lesions. *Arterioscler Thromb Vasc Biol*. 2004;24:2391–2396.
84. Kieffer P, Robert A, Capdeville-Atkinson C, Atkinson J, Lartaud-Idjouadiene I. Age-related arterial calcification in rats. *Life Sci*. 2000;66:2371–2381.

Arteriosclerosis, Thrombosis, and Vascular Biology

JOURNAL OF THE AMERICAN HEART ASSOCIATION

Quantification of Calcification in Atherosclerotic Lesions

Catherine L. Higgins, Seth A. Marvel and Joel D. Morrisett

Arterioscler Thromb Vasc Biol. 2005;25:1567-1576; originally published online May 26, 2005;
doi: 10.1161/01.ATV.0000172017.79441.73
Arteriosclerosis, Thrombosis, and Vascular Biology is published by the American Heart Association, 7272 Greenville Avenue, Dallas, TX 75231

Print ISSN: 1079-5642. Online ISSN: 1524-4636